TECHNICAL MEMORANDUM

585

An assessment of the accuracy of the RTTOV fast radiative transfer model using IASI data

Marco Matricardi

Research Department

February 2009

Submitted to IASI special issue of
Atmospheric Chemistry and Physics

European Centre for Medium-Range Weather Forecasts
Europäisches Zentrum für mittelfristige Wettervorhersage
Centre européen pour les prévisions météorologiques à moyen

Series: ECMWF Technical Memoranda
A full list of ECMWF Publications can be found on our web site under:
http://www.ecmwf.int/publications/

Contact: library@ecmwf.int

European Centre for Medium Range Weather Forecasts
Shinfield Park, Reading, Berkshire RG2 9AX, England

Abstract.

IASI measurements of spectral radiances made between the the 1st April 2008 and the 15th April 2008 are compared with simulations performed using the RTTOV fast radiative transfer model utilizing regression coefficients based on different line-by-line models. The comparisons are performed within the framework of the European Centre for Medium-Range Weather Forecasts Integrated Forecasting System using fields of temperature, water vapour and ozone obtained from short-range forecasts. Simulations are performed to assess the accuracy of the RTTOV computations and investigate relative differences between the line-by-line models and the quality of the spectroscopic databases on which the RTTOV coefficients are based.

1. Introduction

The exploitation of satellite radiance data for Numerical Weather Prediction (NWP) requires the use of an accurate and fast radiative transfer (RT) model to simulate radiances from an input atmospheric profile. The high spectral resolution of radiances measured by the Atmospheric Infrared Sounder (AIRS) (Aumann et al., 2003) on the Earth Observing System (EOS) Aqua platform and the Infrared Atmospheric Sounding Interferometer (IASI) (Chalon et al., 2001) on the MetOp–A platform provides temperature and constituent profiles at a higher accuracy and with more vertical resolution than the conventional filter wheel radiometers. The assimilation of AIRS and IASI long-wave temperature sounding channels at ECMWF has produced a significant positive impact on forecast quality (McNally et al., 2006; Collard and McNally, 2008) and in the near future the use of IASI data could be extended to other spectral bands. The variational approach to the assimilation of these datasets into the ECMWF four-dimensional variational analysis scheme, 4D-Var (Rabier et al., 1998), involves the definition of the observation-error covariance matrix that is used to specify errors associated with radiance data. The observation-error covariance matrix is the sum of the instrumental-error covariance matrix and the forward-model-error covariance matrix which is based on the estimation of errors associated with fast RT models. The low noise level of IASI and AIRS makes RT errors an important contribution to the definition of the observation-error covariance matrix and consequently they must be properly evaluated and their origin fully understood.

Fast RT model errors are dominated by two main components: the parameterization used for the atmospheric transmittances and the errors associated with the spectroscopic parameters and the computational procedures adopted in the line-by-line (LBL) models on which fast RT models are generally based. The fast RT model used operationally at the European Centre for Medium-Range Weather Forecasts (ECMWF) is the Radiative Transfer Model for TOVS (RTTOV) (e.g. Saunders et al. 1999; Matricardi et al. 2004). In RTTOV the transmittances of the atmospheric gases are expressed as a function of profile-dependent predictors. This parameterization of the transmittances makes the model computationally efficient and thus fulfils the NWP requirement of near real-time monitoring and assimilation of satellite radiance data. In fact, LBL models are too computationally expensive to be used in an NWP operational environment. In this paper we give a brief review of the current status of the RTTOV model and discuss the main features of the LBL models that have been used to derive the RTTOV coefficients for IASI focusing on the aspects that distinguish one model from another.

Errors associated to the RTTOV transmittance parameterization for the IASI channels are discussed in detail in Matricardi (2003) and Matricardi (2008) whereas LBL model errors have been investigated in several studies (e.g. Rizzi et al. 2002; Tjemkes et al 2003; Matricardi 2005) using high-spectral resolution aircraft data. In this paper we try to assess the absolute accuracy of the RTTOV model as a whole. The availability of

RTTOV regression coefficients based on different LBL models has also offered the opportunity to investigate relative differences between LBL-models and the quality of the spectroscopic databases used in the LBL-model computations. The assessment of the RTTOV accuracy has been carried out by running a number of Integrated Forecast System (IFS) monitoring experiments where IASI spectra simulated by RTTOV have been compared to IASI spectra measured during the period 1st April 2008-15th April 2008 using short range operational forecasts of temperature, water vapour and ozone fields to specify the RTTOV input state vector.

2. The RTTOV model

The RTTOV model was originally developed at ECMWF (Eyre, 1991) to retrieve temperature and humidity profiles from the Television InfraRed Observation Satellite (TIROS-N) Operational Vertical Sounder (TOVS) (Smith et al., 1979). Subsequently the code has gone through several developments (e.g. Saunders et al. 1999; Matricardi et al., 2004), more recently within the EUMETSAT NWP Satellite Application Facility (SAF), of which RTTOV-9 is the latest version (Saunders et al., 2008). RTTOV covers the spectral range 3-20 microns in the infrared and the frequency range 10-200 GHz in the microwave and supports a large number of platforms and sensors with updates as new sensors are launched. An important feature of the RTTOV model that is essential for use in a NWP environment is that it not only performs the fast computation of the forward (or direct) radiances but also the fast computation of the gradient of the radiances with respect to the state vector variables for the input state vector values (i.e. temperature, variable gas concentrations, cloud and surface properties).

The model uses the polychromatic form of the radiative transfer equation (i.e. the use of channel averaged transmittances in the radiative transfer equation is based on the assumption that this is equivalent to the convolution of the monochromatic radiances) (see Matricardi et al., 2004, for details). The polychromatic approximation is adequate when channels are narrow enough that the convolution of the Planck function can be replaced with its value at the central wave number of the channel. For IASI and AIRS channels the polychromatic approximation results in errors typically below 0.05 K whereas for broad channels the accuracy is generally poor and can result in biases of ~1-2K (Brunel and Turner, 2003). The RTTOV fast transmittance scheme uses regression coefficients derived from accurate LBL computations to express the optical depths as a linear combination of profile dependent predictors that are functions of temperature, absorber amount, pressure and viewing angle (Matricardi and Saunders, 1999). The regression coefficients are computed using a training set of diverse atmospheric profiles chosen to represent the range of variations in temperature and absorber amount found in the atmosphere. Regression coefficients for RTTOV are available based on the 43 profile training set described in Matricardi and Saunders (1999), the 52 profile training set described in Chevallier (2000) and, more recently, on the 83 profile training set described in Matricardi (2008) (henceforth we will refer to these training sets as ECMWF_43_P, ECMWF_52_P and ECMWF_83_P respectively). The latter dataset includes variable profiles of carbon dioxide (CO_2), nitrous oxide (N_2O), methane (CH_4) and carbon monoxide (CO) in addition to water vapour (H_2O) and ozone (O_3). The LBL computations for the minor gases that are not allowed to vary in RTTOV are carried out assuming a climatological mean profile (see next section for details).

The RTTOV-9 fast transmittance algorithm supports a range of predictor sets, namely RTTOV-7 predictors, RTTOV-8 predictors and RTTOV-9 predictors. The selection of the predictors is made according to the coefficients file supplied to the program. The RTTOV-8 predictors (Matricardi et al., 2004) allow to vary the amounts of H_2O, O_3 and optionally CO_2 whereas the RTTOV-9 predictors (Matricardi, 2003) allow to vary

the amounts of H_2O, O_3, CO_2, N_2O, CH_4 and CO. Coefficients based on RTTOV-9 predictors can only be used for AIRS and IASI and input profiles for CO_2, N_2O, CH_4 and CO are mandatory. In addition, RTTOV-9 predictors can be used to compute optical depths for the long atmospheric paths involved in the computation of TOA radiances if solar radiation is required to be included in the short-wave infrared channels (Matricardi, 2003).

Regression coefficients are computed separately for all gases with fixed amounts and for each species that is allowed to vary. Since the convolution of the transmittance of all the gases differs from the product of the transmittance of the single gases convolved individually, effective transmittances are derived that allow Beer's law to be obeyed to a very good approximation (Matricardi, 2003). The accuracy of the fast model transmittance parameterization can be assessed by comparing the transmittances and radiances computed by the fast model with the corresponding values from LBL models in different ways. Firstly, the fast model transmittance profiles and top of the atmosphere (TOA) radiances computed for the regression training data set can be compared with LBL model equivalents to determine the accuracy of the fast model itself. Secondly, a set of profiles independent of the regression coefficients can be used to allow uncertainties from different type of profiles to be included. The accuracy of the RTTOV-9 predictors is discussed in detail in Matricardi (2008). Results for an independent profile set show that the root mean square (rms) of the difference between fast model and LBL radiances is below 0.15K for the vast majority of the channels. Larger errors are observed in spectral regions that see the presence of medium strength water vapour lines, in the ozone band at 9.8 microns and in regions where H_2O lines interfere with absorption lines of other gas species. Results for RTTOV-8 predictors are similar (Matricardi et al., 2004). If we use this error figure as representative of errors associated with the RTTOV fast transmittance parameterization then we can reasonably assume that the RTTOV accuracy is largely determined by the accuracy of the LBL algorithm. For instance the inaccurate knowledge of molecular line strengths alone can result in TOA radiance errors as large as 0.3-0.4 K.

In the infrared domain RTTOV-9 can compute radiances in the presence of clouds and aerosols using a parameterized multiple scattering scheme that allows the polychromatic form of the radiative transfer equation to be retained (Matricardi, 2005). A solar contribution can also be included in the short wave channels (2000-2760 cm^{-1}) for values of the solar zenith angle as large as 84° (Matricardi, 2003). To improve the accuracy of the radiance computation, RTTOV-9 uses a new parameterization of the Planck function based on the linear-in-τ assumption that the source function throughout an atmospheric layer is linear with the optical depth, τ, of the layer and an altitude dependent correction to the local path that takes into account the curvature of the Earth and its surrounding atmosphere. Finally, to compute the infrared emissivity over water a fast surface emissivity routine, ISEM, (Sherlock, 1999) is used.

3. The line-by-line models

As discussed in the previous section, the RTTOV fast transmittance algorithm uses regression coefficients obtained from LBL transmittance calculations. As noted in Rizzi et al. (2001) and Matricardi (2007) LBL model errors tend to be dominated by insufficient knowledge of basic spectroscopy rather than by the computational procedures used in the codes. Spectroscopic errors are of paramount importance for high-resolution sounders like AIRS and IASI that allow the use of channels placed between spectral lines. These channels have weighting functions that are sharper than the weighting functions that characterize the channels placed on top of the spectral lines and consequently particular attention must be paid to the spectral line shape of species like H_2O and CO_2 for which optical depths in the atmosphere can reach very large

values. The effect of line mixing (i.e. the change in line shape due to the redistribution of radiation in overlapping spectral lines) in the CO_2 Q-branches is now routinely incorporated in LBL algorithms and in the recent past progress has been made in the development of improved CO_2 line shapes by taking into account the effect of line mixing in CO_2 P/R-branches. Progress in the development of improved H_2O line shapes is still hindered by the difficulty of achieving good measurements of H_2O amounts in the atmosphere and in the laboratory and the nature of water vapour continuum absorption and its effect on atmospheric radiance is an outstanding and unresolved issue. In LBL models water vapour continuum is usually parameterized using the semi-empirical CKD model by Clough et al. (1989). This model has been recently revised based on the assumption that the continuum absorption in water vapour bands is dominated by the collision-induced absorption resulting from the generation of a short-lived complex of water vapour and colliding molecules (MT_CKD model). Finally, the accuracy of the LBL computations is still significantly affected by the accuracy of laboratory measurements of molecular line strengths.

RTTOV regression coefficients for IASI are available based on various LBL models. Regression coefficients based on version 4 of the GENLN2 LBL model (GENLN2_v4) and version 11.1 of the LBLRTM LBL model (LBLRTM_v11.1) have been generated at ECMWF using RTTOV-9 predictors whereas coefficients based on version 1.11 of the kCARTA LBL model (kCARTA_v1.11) have been generated at Meteo France (Brunel, 2008) using RTTOV_8 predictors. A description of the LBL models is given in the following sections.

3.1 GENLN2_v4

GENLN2_v4 (Edwards 1992) is a line-by-line atmospheric transmittance and radiance model. Line strengths and half-widths are adjusted to the path pressure and temperature and Doppler broadening of the spectral lines is taken into account. To describe the effects of pressure and Doppler line broadening, GENLN2_v4 adopts the Voigt line shape. The GENLN2_v4 CO_2 line shape includes the effect of line mixing and takes into account the sub-Lorentzian behaviour in the far-wing of the line. If data is available, CO_2 Q-branch line mixing in the *υ2* and *υ3* band can be included out to an arbitrary 10 cm^{-1} from line centre. For greater distances from the centre the line shape is approximated by the empirical model by Cousin et al. (1985). This model explains the sub-Lorentzian nature of the CO_2 far wing line shape in terms of duration of collision effects and uses a temperature dependent χ-factor to adjust the standard line shape function based on the impact theory. If no line-mixing data is available then the sub-Lorentzian line shape is used everywhere. The standard release of GENLN2_v4 includes the water vapor continuum model CKD_2.1. However, we carried out our computations using the model CKD_2.4 that became available at the time the regression coefficients were about to be generated. The pressure-broadened band of N_2 at 2350 cm^{-1} (Menoux at al. 1993) and that of O_2 at 1550 cm^{-1} (Timofeyev and Tonkov, 1978; Rinsland et al., 1989) is included as broadband continuum contribution to the absorption and heavy molecules can me modeled using high-resolution cross-sectional data. In our computations, CO_2 Q-branch line mixing has been fully accounted for using first order line-mixing coefficients from Strow et al. (1994).

3.2 kCARTA_v1.11

The kCARTA_v11.1 model (De Souza-Machado et al., 2002) is a fast LBL algorithm where transmittances are computed from compressed look-up tables of atmospheric transmittances (Strow et al., 1998). The look-up tables are computed using a LBL model developed at the University of Maryland, Baltimore County (UMBC-LBL) (Strow et al., 2003) and their use in kCARTA results in very fast computation times. The water vapour continuum model (hence after referred to as MTK_CKD_UMBC) is based on the

MTK_CKD_1.0 model. It uses revised values of the spectral density function coefficients based on measurements of AIRS spectra utilizing in-situ data available from the ARM sites (Machado, 2008). Line mixing coefficients for CO_2 are available for 12 P/R-branch bands and 12 Q-branch bands in the short wave and in the long wave. The kCARTA model for the CO_2 line shape is based on the work by Tobin (1996) and Machado et al. (1999). For the P/R-branch it involves an approximation for the combination of line mixing and duration-of-collision effects. Regarding the UMBC-LBL model it should be stressed that it relies on a full treatment of the CO_2 Q- and P/R-branch line mixing and does not use the perturbation theory. Finally, the collision-induced bands of oxygen at 1600 cm^{-1} and nitrogen at 2350 cm^{-1} are incorporated using the model by Thibault et al. (1997) and Lafferty et al. (1996) respectively.

3.3 LBLRTM_v11.1

The LBLRTM line-by-line model (Clough et al., 1992) has been developed at the Atmospheric and Environmental Research Inc. (AER) and is derived from the Fast Atmospheric Signature Code (FASCODE) (Clough et al. 1981). To describe the effects of pressure and Doppler line broadening the Voigt line shape is used at all atmospheric levels with an algorithm based on a linear combination of approximating functions. LBLRTM incorporates the self- and foreign-broadened water vapor continuum model MT_CKD_2.0 (Tobin et. al. 1999) and the collision-induced bands of oxygen at 1600 cm^{-1} and nitrogen at 2350 cm^{-1} are included as broad-band continuum contributions to the absorption using the models by Thibault et al. (1997) and Lafferty et al. (1996) respectively. In LBLRTM the CO_2 line shape includes the effects of line mixing for the P-R-branch and Q-branch in the $\upsilon 2$ and $\upsilon 3$ band using first order line coupling parameters generated using the code by Niro et al. 2005. Since the model by Niro et al. (2055) combines the effects of line mixing and duration of collision effects, the χ factor is set equal to 1. In addition, the CO_2 continuum is computed using the Niro et al. (2005) coupling coefficients with a scaling factor of 0.75 applied to the $\nu 3$-band to agree with AIRS spectra in the $\nu 3$ spectral region. LBLRTM uses temperature dependent cross section data to model the absorption of heavy molecules. The pressure dependence of the cross sections is treated by performing a convolution of the cross section spectrum with an appropriate Lorentz function.

The computation of the LBL transmittances is performed on a grid of vertical levels of fixed pressure for a regression dataset of diverse atmospheric profiles and require the use of appropriate parameters from a molecular database. These details are summarized in Table 1. Note how for kCARTA and GENLN2 the same molecular database has been used although it should be noted that for GENLN2 the use of the Strow et al.(1994) line mixing coefficients requires the use of CO_2 molecular line parameters from the HITRAN_1992 compilation. For the LBLRTM computations we have envisaged a molecular database that blends line parameters obtained from various sources. This is based on the results shown in Matricardi (2006) which suggest that in a number of spectral regions the use of line parameters from different sources can result in a better agreement of simulations with observations. This blended database is largely drawn from HITRAN_2004 (Rothman et al., 2005) and includes updates up to 1/1/2007. However, in the 9.8 micron ozone band we use ozone line parameters from HITRAN_2000 (Rothman et al., 2003) whereas in the spectral region between 1700 and 2400 cm^{-1} we use water vapour line parameters from GEISA_2003 (Husson et al., 2005). Although Matricardi (2006) suggests that the use of CO_2 line parameters from GEISA_2003 could also be envisaged in the 15 micron CO_2 band, the use of Niro et al. (2005) line mixing coefficients requires that line parameters for CO_2 are obtained from the HITRAN_2000 compilation. From Table 1 it can also be seen that regression coefficients are based on different profile training sets and that all the computations have been performed on the 101 level vertical grid specified by the AIRS science team (Strow et al., 2003).

Table 1: The regression coefficients used for the RTTOV simulations

Coefficients	Continuum	CO2 line mixing	Molecular Database
LBL model: kCARTA Number of levels: 101 Profile training set: ECMWF_52_P	MTK_CKD_v1.1_UMBC	P/Q/R branch (u2 and u3 band)	HITRAN_2000
LBL model: GENLN2 Number of levels: 101 Profile training set: ECMWF_43_P	CKD_v2.4	Q branch (u2 and u3 band)	HITRAN_2000
LBL model: LBLRTM Number of levels: 101 Profile training set: ECMWF_83_P	MTK_CKD_v1.4	P/Q/R branch (u2 and u3 band)	HITRAN_2000 HITRAN_2004/2006 GEISA_2003

For the interpretation of the results we find it useful to include two figures where differences between the various water vapour continuum models are illustrated. In particular, in Fig. 1 we show the water vapour broadening coefficients for the self continuum while in Fig. 2 we show the broadening coefficients for the foreign continuum (self broadening due to H_2O-H_2O collisions is the dominant source of continuum in the window regions whereas foreign broadening due H_2O-N_2 collisions dominates in the water vapour band). These figures show that in the 10 micron window region MTK_CKD_UMBC self broadening coefficients are smaller than CKD_2.4 and MTK_CKD_v1.4 coefficients. In the centre of the water vapour band around 1600 cm^{-1} the CKD_2.4 foreign broadening coefficients are smaller that MTK_CKD_UMBC and MTK_CKD_v1.4 coefficients whereas for larger wave numbers MTK_CKD_UMBC foreign broadening coefficients are larger than CKD_2.4 and MTK_CKD_v1.4 coefficients.

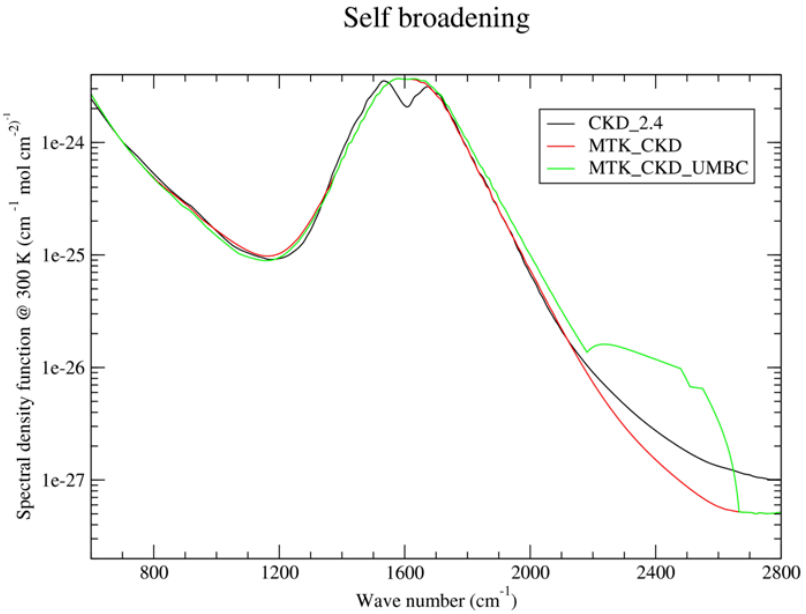

Figure 1: Spectral density function for the water vapour self broadening coefficients at 300K and 1013 hPa.

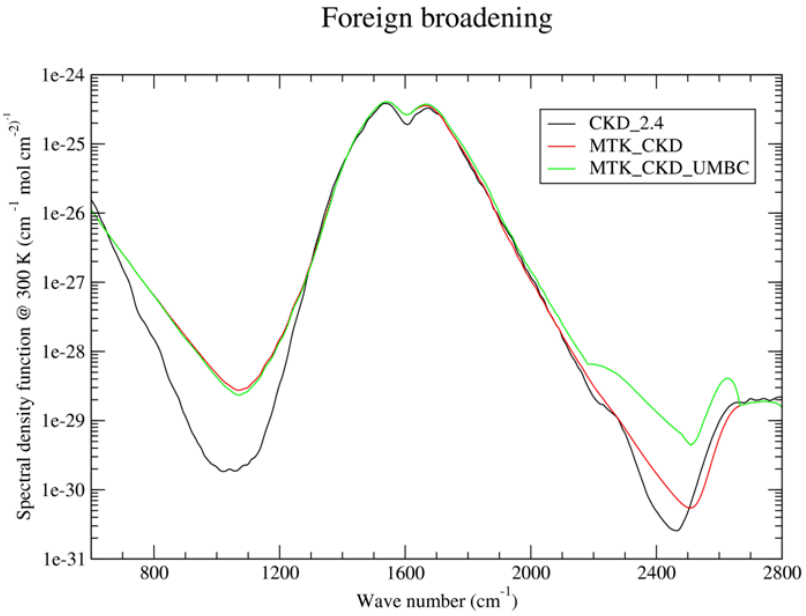

Figure 2: Spectral density function for the water vapour foreign broadening coefficients at 300K and 1013 hPa.

All LBL datasets include N_2, O_2, HNO_3, OCS, CCl_4, CF_4, CCl_3F and CCl_2F_2 among the gases with fixed amount. Regression coefficients based on the GENLN2 and LBLRTM models allow the variation of CO_2, N_2O, CO, and CH_4 amounts whereas in kCARTA the amount of these gas species is fixed. The LBLRTM dataset includes an additional number of fixed gas species, i.e. NO_2, SO_2 and NO. In general, atmospheric constituent profiles for all gases are based on AFGL profiles scaled to reflect present-day concentrations. However, in the LBLRTM dataset we have used HNO_3 and NO profiles generated using the MOZART chemical transport model (Clerbaux, 2008) whereas in the kCARTA dataset the concentrations of CO_2, N_2O, CO and CH_4 are based on the climatological profiles described in Matricardi (2003).

4. The monitoring experiments

Three baseline monitoring experiments have been run using cycle 33R1 of the IFS (which was the operational cycle from June until October 2008) using the T799 horizontal truncation. This truncation corresponds to a horizontal resolution of ~25 km. A feature of cycle 33R1 of the IFS is a vertical discretization of the atmosphere into a grid of 91 pressure levels. The model uses a hybrid vertical coordinate with coordinates that follow the orography of the terrain in the lower troposphere and pressure coordinates in the stratosphere above about 60 hPa. The top level is fixed at 0.01 hPa (about 80 km) and of the 91 levels in the vertical, 52 are above 100 hPa. The state vector variables used in the RTTOV simulations are forecast fields of temperature, humidity, ozone and surface parameters. IASI data within a 12-hour 4D-VAR window are grouped into 30 minutes time slots. A T799 high resolution forecast is then run from the previous analysis and observation minus model differences are computed for IASI soundings within a given time slot. This sequence is then repeated for each 12-hour 4D-VAR window. In this study we consider IASI data inside 12-hour 4D-VAR windows during the period 1st April 2008-15th April 2008. The statistics of the difference between global radiosonde observations and ECMWF analyses in the troposphere show values of the standard deviation typically between 0.5K and 1K for temperature and between 0.5 and 1.5 g/Kg for water vapour. In the stratosphere, standard deviations for temperature can reach 1.5 K. Ancillary data used in the RTTOV computations include sea-surface temperature (SST). SST fields in cycle 33R1 are based on

analyses received from the National Centers for Environmental Prediction (NCEP), Washington, DC, on a 0.5° x 0.5° grid. These analyses are based on ship, buoy and satellite observations. The SST root mean square error (rms) relative to buoy observations is ~0.36 K (Kara et al., 2006). However, this figure can be significantly different in shallow waters where rapid changes due to the upwelling radiation can occur close to land.

Since the the RTTOV optical depth computations are defined by the number of levels in the coefficient file, the IFS pressure levels must be interpolated to the same levels as the coefficient files. To this end we have used the RTTOV-9 new internal interpolation scheme that allows the input profile to be defined by the user. However, it should be noted that although RTTOV computes optical depths on the levels specified in the coefficient files, the integration of the RT equation is performed on the 91 IFS levels. To ensure that the Jacobians are properly mapped back on the user levels, the optical depths must be interpolated to the IFS levels using the same interpolation scheme utilized for the atmospheric variables.

The IASI spectra used in our experiments are measured over the sea. To reduce the amount of data we have sub-sampled by arbitrarily selecting one out of eleven scan-positions. This also ensures that for two adjacent scan lines we always sample two different scan positions. Only channels detected as clear by the ECMWF cloud detection algorithm are processed. Since the ECMWF cloud detection algorithm (McNally and Watts 2003) finds clear channels rather than clear locations, the size of sample varies with the sensitivity of the channel to clouds. Channels characterized by weighting functions that peak at high altitudes are less sensitive to clouds than channels with weighting functions that peak at low altitudes or at the surface. To illustrate this, in Fig. 3 we show the size of the sample for each channel in three latitude bands. It can be clearly seen that the size of the sample varies from several thousands spectra for the channels peaking at middle and high altitudes to a few thousands for channels peaking at low altitudes or at surface. To avoid reflected solar radiation and non-LTE effects (the latter are not modelled in RTTOV), in the spectral region between 2000 and 2760 cm^{-1} we have sampled only night-time spectra. This is reflected in Fig. 3 where the size of the

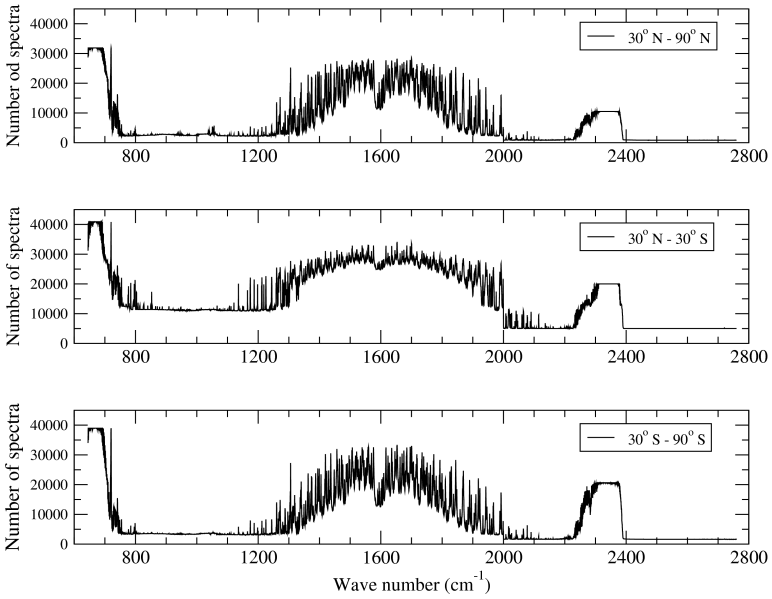

Figure 3: The number of spectra sampled as clear for each IASI channel for three different latitude bands.

sample in this spectral region is significantly smaller than the size of the sample in other spectral regions. Note that to exclude night-time spectra we have used the criterium that the local solar zenith angle is greater than 100°. This means that a given location can be considered not to be in daylight up to an altitude of ~100km (i.e. the altitude above which we consider the atmosphere to be transparent in our calculations).In our RTTOV computations the state vector includes profiles of temperature, water vapour and ozone, surface parameters (e.g. skin temperature and surface pressure) and a wave number dependent value of the sea surface emissivity that includes the dependence on the viewing geometry. In addition to the profiles of temperature, water vapour and ozone, the experiments that use RTTOV coefficients based on GENLN2 and LBLRTM also require input profiles of CO_2, CO, N_2O and CH_4. Since profiles for these trace gases are not prognostic variables in the ECMWF model we had to fix the amounts in the GENLN2 and LBLRTM experiments. To this end we have chosen the values assumed in the LBL computation used to train kCARTA. The rationale behind this choice is that at present kCARTA coefficients are used operationally at ECMWF for the assimilation of AIRS and IASI radiances and we want to use the kCARTA spectra as benchmark in our comparisons.

5. Discussion of the Results

5.1 IASI band 1 (645 to 1200 cm^{-1})

In Fig.4 we show the mean value of the difference (bias) between observed and simulated radiances in units of equivalent black body brightness temperature for the latitude band between 30º N and 90º N for IASI band 1. In the top panel the LBLRTM spectrum (solid red line) is superimposed on the kCARTA spectrum (solid black line) whereas in the bottom panel the GENLN2 spectrum (solid red line) is superimposed on the kCARTA spectrum.

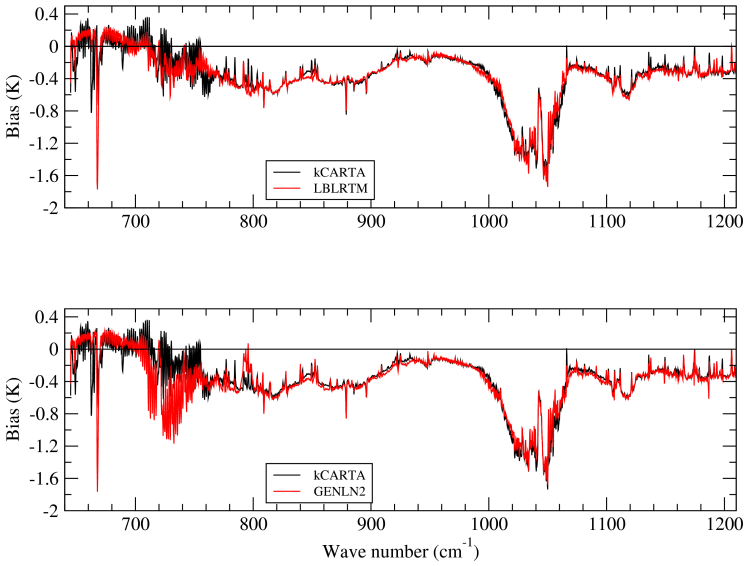

Figure 4: The mean value of the difference between observed and computed brightness temperatures in the northern hemisphere for IASI band 1.

Fig.4 shows that for all experiments biases are generally within ±1K in all spectral regions. The only exception is the ozone band at 9.8 microns where biases can reach 1.5 K. Of particular interest are the result obtained in the 15 microns temperature sounding CO_2 ν2 band where the GENLN2 experiment shows

significantly larger biases between 700 cm^{-1} and 750 cm^{-1}. To interpret this result we should bear in mind that, as discussed in section 3, GENLN2 uses the Cousin et al. (1985) empirical model to describe the far-wing shape of the CO_2 line shape. The χ-factor used in the $\nu 2$-band is based on spectra measured in the $\nu 3$-band. However, the symmetry of the 4.3 microns bands is different from the symmetry of the 15 microns bands and consequently the component of the χ factor due to line mixing is in error and the effect of line-mixing will be over-estimated in GENLN2. Results shown in Fig.4 show that errors in the CO_2 line shape can significantly degrade the accuracy of the spectra. A feature of the LBLRTM and GENLN2 spectra is the large bias (1.8K) seen in correspondence to the CO_2 Q-branch at 667 cm^{-1}. Since GENLN2 and LBLRTM use line mixing coefficients based on a 1st order perturbation theory, it would appear that this is not adequate for the 667 cm^{-1} Q-branch. The formulation of the line mixing model could also explain the very close similarities between the LBLRTM and GENLN2 spectra and the differences between these two models and kCARTA in the 645 to 700 cm^{-1} spectral region. These differences cannot be attributed to the molecular parameters since, for instance, LBLRTM and kCARTA use the same HITRAN_2000 compilation. It should also be noted that in this spectral region a consistent number of channels is sensitive to emission at high altitudes and consequently can be affected by systematic temperature errors of the ECMWF model in the upper stratosphere and mesosphere. As discussed above, the performance of GENLN2 between 700 to 750 cm^{-1} can be explained in terms of the different treatment of the far-wing CO_2 line shape. In the same spectral region kCARTA and LBLRTM spectra show similar features with differences not larger than 0.2K. However, the kCARTA spectrum is more irregular than the LBLRTM spectrum. This behaviour can be explained by factors that include the line mixing model, uncertainties in the temperature profile and errors in the strengths and widths of the weak water vapour lines originating from the edge of the water vapour pure rotational band. The errors in the line strengths and widths can either be due to uncertainties in the water vapour profile or due to spectroscopic errors (in addition to this kCARTA and LBLRTM use different water vapour molecular databases). It should also be stressed that in the experiments CO_2 amounts are not varied and that a fixed climatological profile is used in the RT computations. Spectra in the window region between 800 and 1200 cm^{-1} and in the ozone band are remarkably close. All experiments show very similar negative biases (i.e. the radiances are overestimated). In the window regions they vary between -0.1 and -0.6K whereas in the ozone band they can reach values as large as -1.6K. Small differences also exist between the spectra obtained in the latitude band between 30°S and 90°S (Fig.6) although biases between 800 and 1080 cm^{-1} are smaller compared to those obtained in the northern hemisphere. Also noticeable is the feature (a kink) in the GENLN2 spectrum around 1000 cm^{-1}. The absorption in the window region between 800 and 1200 cm^{-1} is primarily due to water vapour and consists mainly of the absorption due to water vapour self-continuum although in the high-wavenumber boundary of the window the contribution of weak water vapour lines originating in the $\upsilon 2$-band has also to be taken into account. With the exception of a few channels, the specification of the continuum model and the choice of the molecular parameters do not appear to have a significant impact on the spectra obtained at mid and high latitudes. The absorption due to the water vapour self continuum is proportional to the square of the water vapour amount and for a fixed amount of water vapour it decreases with temperature. In general, the colder air masses typically encountered at mid-high latitudes are associated with less water vapour and the competing effect of temperature and water amount is stronger than in the much more humid conditions encountered in the tropical regions. Errors in the temperature profiles and, above all, errors in the water vapour profiles in the lower troposphere and near the surface can then affect the simulated spectra in various measures and result in the different biases observed at different latitudes. Errors in the SST analysis should also be taken into account in that they can contribute to

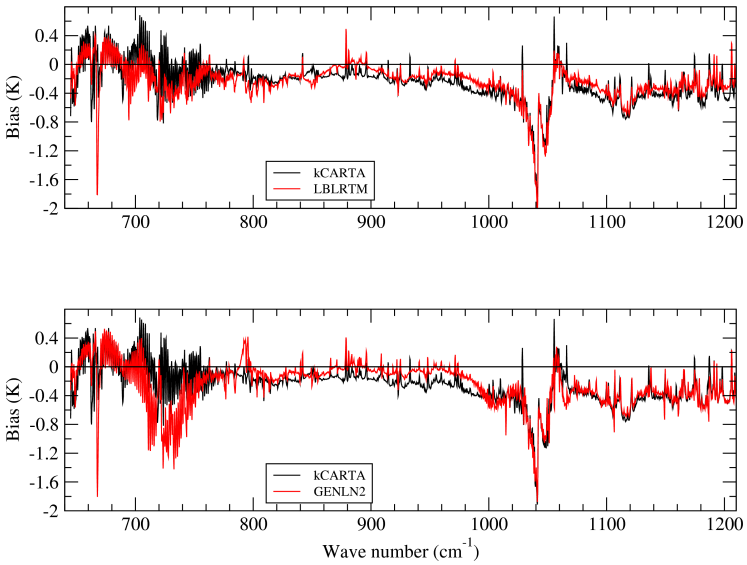

Figure 5: The mean value of the difference between observed and computed brightness temperatures in the tropical region for IASI band 1.

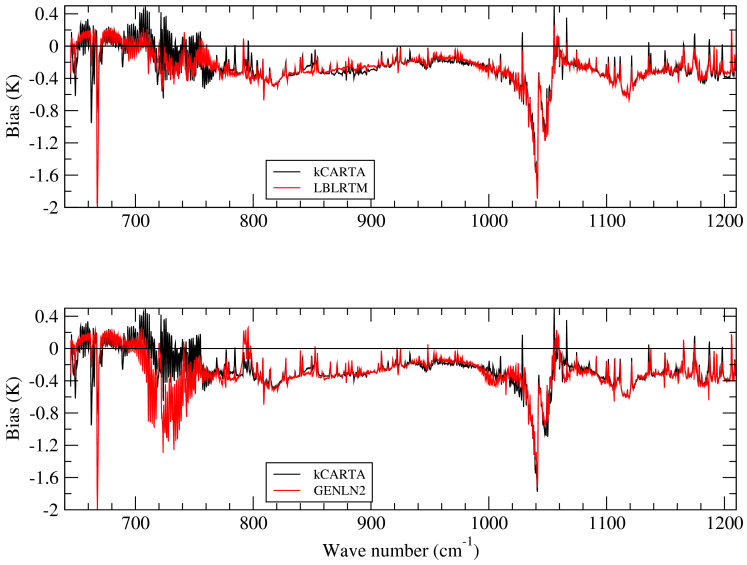

Figure 6: The mean value of the difference between observed and computed brightness temperatures in the southern hemisphere for IASI band 1.

the biases. In addition, they indirectly affect the values of the sea surface emissivities computed by ISEM since ISEM does not take into account the temperature dependence of the water vapour optical parameters. However, since the SST is used as the skin temperature in the RT computations, the larger biases in the northern hemisphere cannot be explained in terms of SST alone since this feature should also be present in the high-wavenumber boundary of the window region (i.e. between 1100 and 1200 cm^{-1}). It is also possible that channels identified by the cloud detection scheme as clear channels are in fact channels affected by clouds. The negative sign of the biases (i.e. the RT model overestimates the radiances) is consistent with this hypothesis. However, results obtained using aircraft data in controlled clear-sky conditions (e.g. Matricardi,

2007) show biases whose magnitude is similar to that obtained in our study. If we assume that these biases are attributable to the water continuum then the effect due to errors in the cloud detections scheme must be very small. Of course, we cannot rule out that we are observing biases that are the result of the competing effect of various factors. Biases observed in the ozone band are probably dominated by spectroscopic errors although the larger values obtained in the northern hemisphere might reflect a poor performance of the ozone assimilation system. Results for the tropical band (30°N-30°S) are shown in Fig. 5. where it can be seen that in contrast to the previous cases differences now exist between the spectra in the window regions.

This is a direct consequence of the fact that the high tropical water vapour column concentrations make the water vapour continuum absorption a much more important factor. To exemplify this we have run a further experiment where the kCARTA spectra have been computed using the same water vapour continuum model used in the LBLRTM model. The results are shown Fig.7 where we have plotted the difference between the standard kCARTA mean spectrum and the LBLRTM mean spectrum (top panel) and the difference between the modified kCARTA mean spectrum and the LBLRTM mean spectrum (bottom panel).

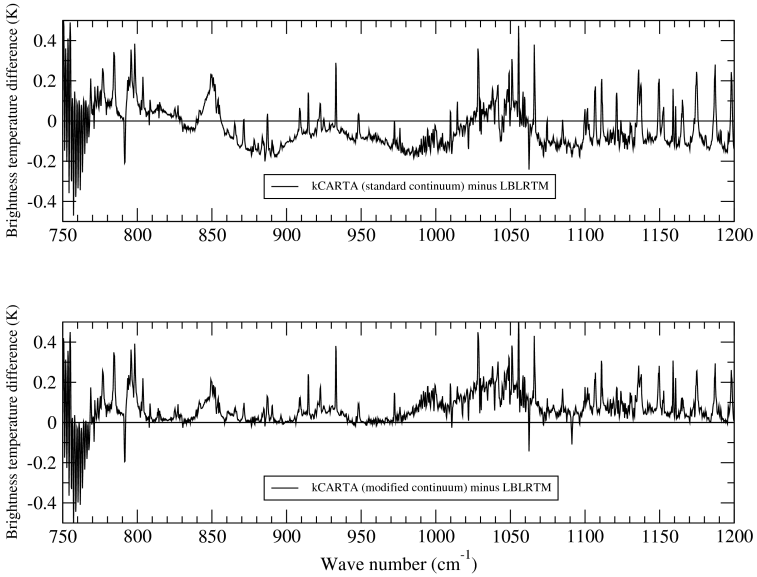

Figure 7: The difference between a) kCARTA and LBLRTM in the tropical region; b) kCARTA_LBL and LBLRTM in the tropical region.

Fig.7 shows that the use of the same continuum model greatly reduce the differences between the spectra. This is all the more evident between 800 and 980 cm^{-1}. The residuals seen in correspondence of the $CFCl_3$ band at 846 cm^{-1} and the CF_2Cl_2 band at 923 cm^{-1} are attributable to the different amounts used for these molecules in kCARTA and LBLRTM whereas residuals around 880 cm^{-1} should be attributed to the spectroscopy. In the window region between 1080 and 1200 cm^{-1} the change in the continuum reduces the peak-to-peak differences and shifts the biases towards positive values. This would suggest that in this spectral region differences between the spectra are attributable primarily to differences between the molecular databases. Results shown in the bottom panel of Fig.7 corroborate this hypothesis in that GENLN2 and kCARTA biases are in very good agreement (they use the same HITRAN_2000 molecular database). Finally, we want to comment on the feature around 1000 cm^{-1} seen in the GENLN2 spectra for the tropical and southern latitude band. This feature is not present in the kCARTA and LBLRTM experiments and its origin is difficult to interpret. In this spectral region, the only obvious difference between GENLN2 and the other LBL models is the much smaller value of the foreign broadening spectral density function but it is

difficult to argument in favour of a possible impact of the foreign continuum since foreign broadening should not be important at these wave numbers.

5.2 IASI band 2 (1200 to 2000 cm^{-1})

Results for IASI band 2 in the northern hemisphere are shown in Fig. 8. Biases vary between -0.8 and 0.8K although larger values up to -1.4K are observed for channels located in the spectral region characterized by the presence of the strong ν4-band of methane at 1310 cm^{-1}. The same spectral region is characterized by large negative biases. This can be partly explained by the fact that methane amounts are fixed to climatological values. LBLRTM and kCARTA spectra exhibit very similar features in the left side and central part of the water vapour ν2 band from 1400 up to 1700 cm^{-1}. To the right side of the band the structure of the spectra is more irregular and in the case of kCARTA we can observe a consistent number of spikes that are not present in the LBLRTM spectrum. The GENLN2 spectrum in the lower panel shows larger biases around 1600 cm^{-1}, a feature we attribute to the water vapour continuum model that in the case of GENLN2 (see Fig. 2), uses smaller values of the spectral density function in this region. Between 1400 and 1700 cm^{-1} the GENLN2 spectrum is more irregular and probably reflects differences in the spectroscopy whereas between 1700 cm^{-1} and 2000 cm^{-1} it follows more closely the LBLRTM spectrum. In terms of absolute biases, results obtained in the southern hemisphere (shown in Fig. 10) are comparable to those obtained in the northern hemisphere with the exception of the region between 1980 and 2000 cm^{-1} where the LBLRTM spectrum exhibits larger biases. Results for the tropical band are shown in Fig. 9. All the spectra are characterized by larger biases that, with the exception of channels in the methane band where values can reach -2K, vary between -0.8 and 1K. Differences between the spectra are now larger and the structure of the spectra is more articulate. It would appear that LBLRTM tends to fit better the observations although it is difficult to give a conclusive answer since the results can be affected by uncertainties in the water vapour profiles above all in presence of the high water vapour loadings characteristic of tropical conditions.

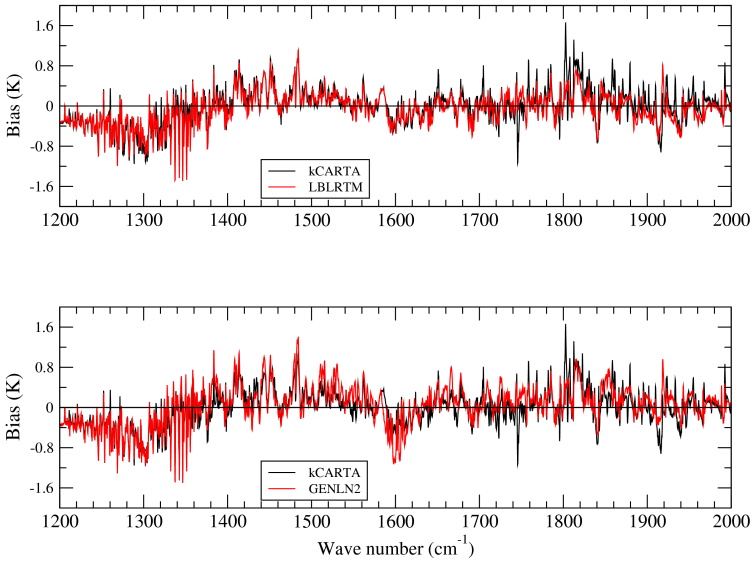

Figure 8: The mean value of the difference between observed and computed brightness temperatures in the northern hemisphere for IASI band 2.

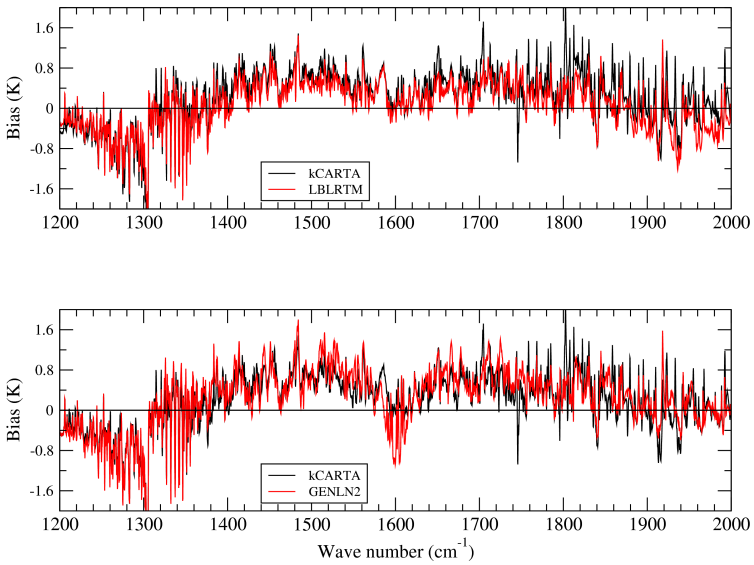

Figure 9: The mean value of the difference between observed and computed brightness temperatures in the tropical region for IASI band 2.

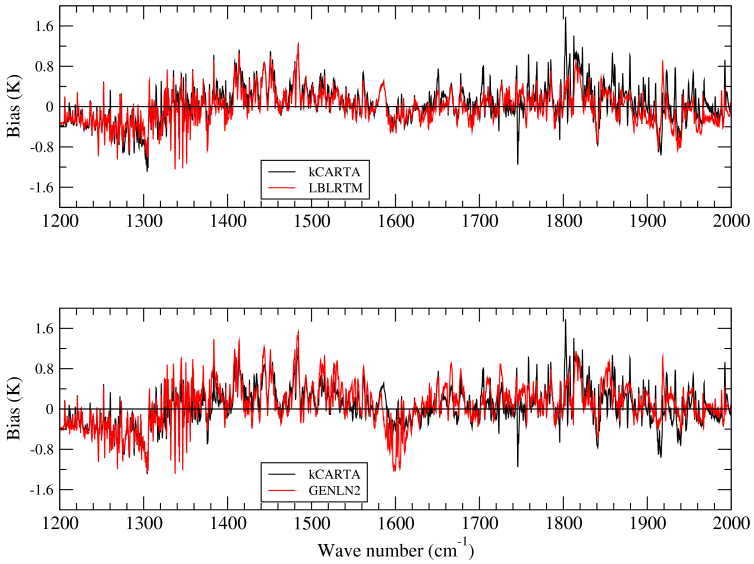

Figure 10: The mean value of the difference between observed and computed brightness temperatures in the southern hemisphere for IASI band 2.

Since GENLN2 and kCARTA use the same molecular database it is difficult to explain the origin of the large spikes in the kCARTA spectra since these cannot attributed to the continuum model as shown in the upper panel of Fig. 11. In this panel, we have plotted the difference between the standard kCARTA spectrum and the kCARTA spectrum computed using the LBLRTM continuum (kCARTA_LBL). It shows that in IASI band 2 differences between the kCARTA and LBLRTM continuum can only have a significant impact in the regions at centre and at the edges of the band, hence the continuum cannot be responsible for the spikes in kCARTA. It could be argued that the kCARTA spikes can be a feature of the fast transmittance model used in RTTOV. However, in IASI band 1 and IASI band 2 the predictors used to compute the kCARTA coefficients are the same as those used for the LBLRTM and GENLN2 coefficients. The computation of the water vapour coefficients involve the weighting of the input data prior to the regression

and to our knowledge the details of the procedure used to perform this operation for the kCARTA coefficients does not differ from the procedure adopted for the GENLN2 and LBLRTM coefficients. Finally, in the lower panel of Fig. 11 we have superimposed the spectra that show the difference between the kCARTA mean spectrum and the LBLRTM mean spectrum and the difference between the kCARTA_LBL mean spectrum and the LBLRTM mean spectrum. This also allows us to conclude that differences in the region between 1970 and 1990 cm^{-1} between the spectra of kCARTA and LBLRTM in the southern hemisphere and in tropics are almost entirely attributable to the continuum model.

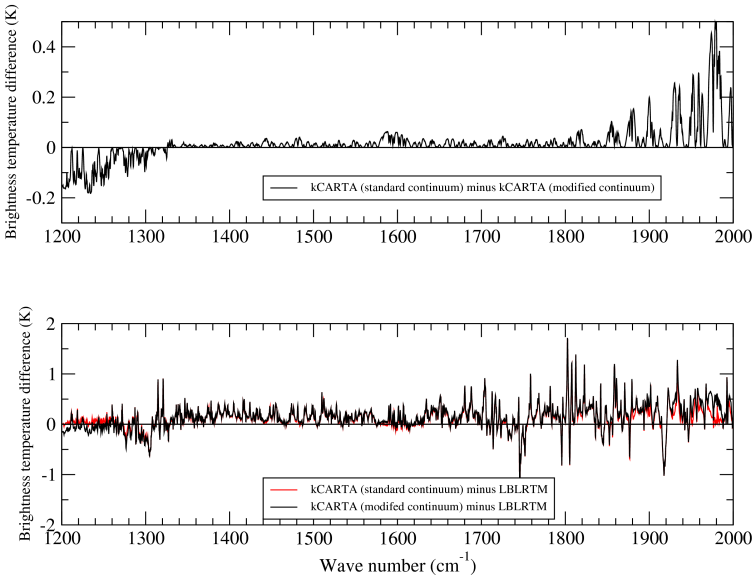

Figure 11: The difference in the tropical between a) kCARTA and kCARTA_LBL; b) kCARTA and LBLRTM (solid black line) and kCARTA_LBL and LBLRTM (solid red line).

5.3 IASI band 3 (2000 to 2760 cm^{-1})

Results for IASI band 3 are shown in Fig. 12, Fig. 13 and Fig. 14 for the northern hemisphere, tropics and southern hemisphere respectively.

Larger biases between 2080 and 2200 cm^{-1} in the southern hemisphere and in the tropics reflect the latitudinal gradients of CO amounts not accounted for in the RT computations. In the same spectral region biases in the northern hemisphere vary between -0.4K and 0.4K. Large spikes in the kCARTA spectra are a noticeable feature between 2000 and 2150 cm^{-1}. In the υ3-CO_2 band between 2200 and 2400 cm^{-1} biases in the northern and southern hemisphere assume negative values that vary between -1.8 and -0.4K. In the tropical region, biases are generally smaller although larger values are observed in the region around 2270 cm^{-1}. In the case of GENLN2 the bias can be as large as -3K. The biases observed in the υ3-band are larger than biases in the υ2- band. The lesser accuracy to which the CO_2 line parameters are known in this spectral region is certainly reflected in the larger biases. However, biases in the ECMWF stratospheric and mesospheric temperature profiles could play an important role in a region with a large number of channels characterized by very high-peaking weighting functions with tails that can extend well into 0.2 hPa. In addition, as a result of the symmetry of the states involved in the molecular transitions, in this same region P/R-branch line mixing is expected to be twice as strong than in the υ2-band and consequently errors in the

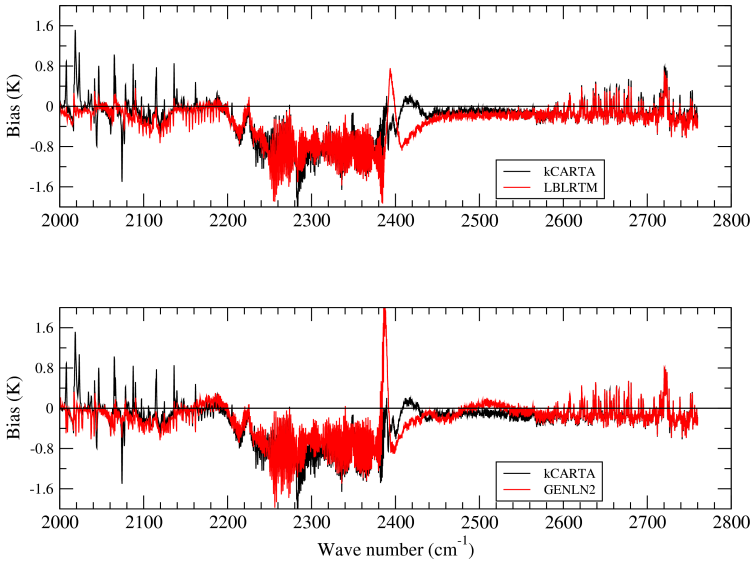

Figure 12: The mean value of the difference between observed and computed brightness temperatures in the northern hemisphere for IASI band 3.

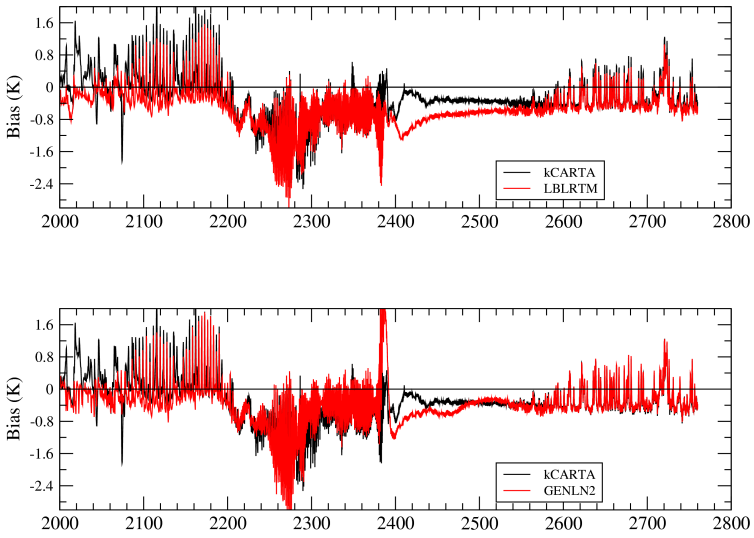

Figure 13: The mean value of the difference between observed and computed brightness temperatures in the tropics for IASI band 3.

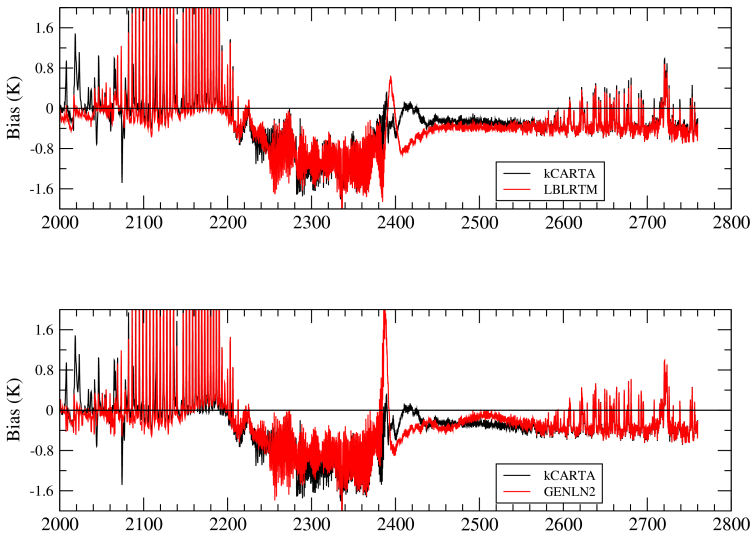

Figure 14: The mean value of the difference between observed and computed brightness temperatures in the southern hemisphere for IASI band 3.

Cousin line shape should affect the GENLN2 spectra. As shown in our plots, GENLN2 spectra in the region between 2380 and 2400 cm^{-1} exhibit biases that are typically 2K larger than in the equivalent kCARTA spectra. If the behaviour of GENLN2 is justified on the grounds of inaccurate line shape, the kCARTA and, to a greater degree, LBLRTM spectra, show that there are still issues with the modelling of CO_2 line shape in the CO_2 υ3-bandhead. In particular, between 2380 and 2400 cm^{-1} the LBLRTM spectra show large oscillations whose amplitude can reach almost 3K in the northern hemisphere. There is still a possibility that this result is due to biases in the ECMWF temperature profiles but we would like to bring forward the hypothesis that this behaviour might be related to the treatment of the CO_2 continuum in LBLRTM. Our spectra could indicate that the scaling factor of 0.75 applied to the CO_2 continuum might not be universally valid. This hypothesis seems to be corroborated by the results obtained by Masiello et al. (2009) using aircraft data. They show that changing the scaling factor to the value used in a previous release of LBLRTM can improve the accuracy of the spectra. In the 2500 cm^{-1} window region differences between the spectra reflect differences between the continua models. The top panel in Fig. 15 shows the difference between kCARTA and kCARTA_LBL and illustrates how the change of the continuum model has an impact between 2380 and 2660 cm^{-1}. The bottom panel shows that the use of the same continuum model has reduced to naught differences between kCARTA and LBLRTM in the 2440 to 2624 cm^{-1} spectral region. Hence, in this spectral region differences between kCARTA and LBLRTM can be attributed solely to the continuum. Beyond 2624 cm^{-1}, differences between the spectra are attributable to the water vapour spectroscopy. This is clearly demonstrated by the fact the kCARTA spectra are in better agreement with the GENLN2 spectra. In the spectral region dominated by the continuum absorption it appears that the kCARTA spectra are in better agreement with observation suggesting that the modifications made to the continuum model have improved the quality of the spectra. Conversely, results in the region dominated by line absorption tend to suggest that the spectroscopic parameters used in LBLRTM fit better the observations.

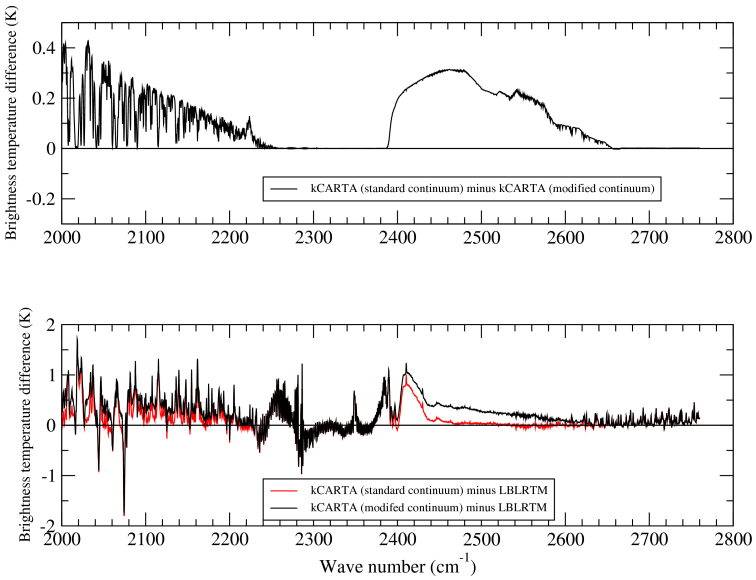

Figure 15: The difference in the tropical between a) kCARTA and kCARTA_LBL; b) kCARTA and LBLRTM (solid black line) and kCARTA_LBL and LBLRTM (solid red line).

6. Conclusions

Four monitoring experiments have been carried out to compare IASI observed radiances to radiances simulated by the RTTOV fast radiative transfer model using regression coefficients based on the GENLN2, kCARTA and LBLRTM LBL models using different molecular databases. Results obtained from IASI data between the 1st April 2008 and the 15th April 2008 using clear channels (i.e. channels not affected by clouds) over the sea show that in the northern and southern hemisphere biases in IASI band 1 and 2 are typically within ±1K. In the tropics, biases in the water vapour ν2- band do increase but for most of the channels the peak-to-peak value is still within within ±1K. The 1K figure is exceeded in the ozone sounding band and in the ν4-methane band. For ozone, the larger biases observed in the northern hemisphere probably reflect a poorer performance of the ozone assimilation system in this region. A more accurate description of the CO_2 line shape that takes into account P/R-branch line mixing and duration of collision effects has a significant impact on the simulated radiances in the CO_2 ν2-band resulting in a reduction of the biases up to 1K. In the same band, line mixing coefficients based on a first order perturbation theory appear not to be adequate to model the absorption in the Q-branch at 667 cm^{-1}. In the water vapour band the use of the MT_CKD water vapour continuum model results in a reduction of the bias of typically 1K in the region around 1600 cm^{-1}. In the window region between 800 and 1000 cm^{-1} differences generated by the use of different continuum models do not exceed 0.2 K whereas absolute biases typically vary between -0.4 and 0K. In the ν2 water vapour band, the LBLRTM spectra do appear to fit better the observations probably due to the use of improved line parameters. On the right side of the water vapour band, we observed a consistent number of spikes in the kCARTA spectra whose origin we were not able to assess. The larger biases observed in the water vapour band tend to reflect errors in line parameters generated by spectroscopic errors and by the inaccurate specification of the water vapour profiles. To this end, it has been suggested that line strengths and temperature dependences of widths used in molecular databases are in error and consequently we encourage LBL developers and users to investigate the use of alternative sets of water vapour line parameters when they become available to the wider community. In IASI band-3 large errors are observed in the CO band that reflect the gradient of CO variation not accounted for in RTTOV. In the important temperature

sounding CO_2 ν3-band we obtained typically negative biases that vary between 0K and -3K. These biases are significantly larger than biases observed in the ν2-band and this certainly reflects the lesser accuracy to which line parameters are known in the ν3-band. However, in this spectral region biases in the temperature profiles can have a significant impact. GENLN2 and LBLRTM exhibit larger biases around 2260 cm^{-1} whereas kCARTA biases are larger around 2300 cm^{-1}. As in the ν2-band, kCARTA and LBLRTM improvements in the CO_2 line shape due to the introduction of P/R-branch line mixing and duration of collision effects is reflected in the smaller biases observed in the CO2 ν3-bandhead. However, the structure of the spectra suggests that there are still issues in this region, above all, for LBLRTM whose spectra, for instance, display large oscillations not seen in the kCARTA. We have tentatively suggested that this behaviour might be due to the treatment of the CO_2 continuum in LBLRTM. An update of the line coupling and continuum model might be required possibly with a revision the CO_2 continuum scaling factor that might not be universally valid. The ν3-band contains a consistent number of very good temperature sounding channels placed in spectral regions where the interference of different absorbing species is minimal. To mitigate the IASI instrument noise in this band, we will study the possibility of exploiting the noise reduction capability of principal component analysis by investigating the assimilation of principal components or the closely related reconstructed radiances in the NWP system. It is then crucial that line mixing coefficients based on updated CO_2 ν3-band line parameters be made available to help reducing errors in this band. Finally, we want to conclude by noting that we are aware of the limitations inherent in the study of RT and spectroscopic errors using an NWP environment. We have stressed, for instance, that systematic profile errors can affect the results. However, an NWP system offers the unique possibility of using a very robust statistical sample made of a large number of data obtained in very diverse conditions. In many instances, results obtained in this study are consistent with results obtained by using aircraft data in very controlled atmospheric situations albeit their interpretation may differ. This encourages us in continuing pursuing this effort above all in the light of the continuous improvements made in NWP.

Acknowledgements

IASI has been developed and built under the responsibility of the Centre National d'Etudes Spatiales (CNES, France). It is flown onboard the Metop satellites as part of the EUMETSAT Polar System. The IASI L1 data are received through the EUMETCast near real time data distribution service. We want to thank P. Brunel (Météo France) for having made available the kCARTA coefficients, C. Clerbaux (Service d'Aéronomie) for having made available concentrations for minor gas species, T. McNally (ECMWF) for the very helpful collaboration received during the set up of the monitoring experiments and A. Collard (ECMWF) and N. Bormann (ECMWF) for the implementation of IASI and RTTOV-9 in the ECMWF data assimilation system.

References

Aumann, H.H., Chahine, M.T., Gautier, C., Goldberg, M.D., Kalnay, E., McMillin, L.M., Revercomb, H., Rosenkranz, P.W., Smith, W.L., Staelin, D.H.,Strow, L.L., Susskind, J.: AIRS/AMSU/HSB on the Aqua mission: design, science objectives, data products, and processing systems, *IEEE Transactions on Geoscience and Remote Sensing*, **41**, Issue 2, 253 – 264, 2003**.**

Brunel, P., and Turner, S.:On the use of Planck-weighted transmittances in RTTOV, *Proceedings of the 13th International TOVS study conference*, Ste Adele, Canada, 2003.

Brunel, P.: Personal Communication, 2008.

Chalon, G., Cayla, F., and Diebel, D.: IASI: An Advanced Sounder for Operational Meteorology, *Proceedings of the 52th Congress of IAF*, Tolouse, France, 2001.

Chevallier, F.:Sampled database of 60-level atmospheric profiles from the ECMWF analyses, *NWP SAF Report* No. NWPSAF-EC-TR-001. (http://www.ecmwf.int/publications/library/do/references/list/202)

Clerbaux, C. :Personal Communication, 2008.

Clough, S.A., Kneizys, F.X., and Davis R.W.: Line shape and the water vapour continuum, *Atmospheric Research,* **23**, 229-241, 1989.

Clough, S.A, Iacono, M.J. and Moncet J.-L.: Line by line calculation of atmospheric fluxes and cooling rates: application to water vapor, *J. Geophys. Res.*, **98**, 15761-15785, 1992.

Collard, A.D., and McNally, A.P.:Assimilation of IASI radiances at ECMWF, *Q. J. Roy. Meteorol. Soc*., in review, 2008.

Cousin, C., Le Doucen, R., Boulet, C., and Henry, H.: Temperature dependence of the absorption in the region beyond the 4.3 μm band head of CO_2. Part 2: N_2 and O_2 broadening, *Applied Optics*, **24**, 3899-3907, 1985.

De Souza-Machado, Strow, L.L., Tobin, D., Motteler, H., and Hannon, S.E.: Improved atmospheric radiance calculations using CO2 p/r-branch line mixing, in *Proc. Euro. Symp. Aerospace Remote Sensing* Europto Series, 1996.

De Souza-Machado, Strow, L.L., Motteler, H., and Hannon, S.E.: kCARTA: an atmospheric radiative transfer algorithm using compressed lookup tables. *Univ. Maryland Baltimore County, Dept. Physics, Tech. Report*, available at http://asl.umbc.edu/pub/rta/kcarta, 2002.

De Souza-Machado, S.:Personal comunication, 2008.

Edwards, D.P.: GENLN2. A general Line-by-Line Atmospheric Transmittance and Radiance Model, *NCAR Technical note* NCAR/TN-367+STR, National Center for Atmospheric Research, Boulder,Co, 1992.

Eyre, J.R.:A fast radiative transfer model for satellite sounding system, *ECMWF Research Dept. Tech. Memo*. 176, http://www.ecmwf.int/publications, 1991.

GLOBALVIEW-CH4: Cooperative Atmospheric Data Integration Project - Methane. CD-ROM, NOAA ESRL, Boulder, Colorado [Also available on Internet via anonymous FTP to ftp.cmdl.noaa.gov, Path: ccg/ch4/GLOBALVIEW], 2008.

GLOBALVIEW-CO: Cooperative Atmospheric Data Integration Project - Carbon Monoxide. CD-ROM, NOAA ESRL, Boulder, Colorado [Also available on Internet via anonymous FTP to ftp.cmdl.noaa.gov, Path: ccg/co/GLOBALVIEW], 2008.

GLOBALVIEW-CO2: Cooperative Atmospheric Data Integration Project - Carbon Dioxide. CD-ROM, NOAA ESRL, Boulder, Colorado [Also available on Internet via anonymous FTP to ftp.cmdl.noaa.gov, Path: ccg/co2/GLOBALVIEW], 2008.

Jacquinet-Husson, N., Scott, N.A., Chedin, A., Garceran, K., Armante,R., Chursin, A.A.,Barbe, A., Birk, M., Brown, L.R., Camy-Peyret, C., Claveau, C.,Clerbaux, C., Coheur, P.F., Dana, V., Daumont, L.,Debacker-Barilly, M.R.,Flaud, J.M.,Goldman, A.,Hamdouni, A.,Hess, M.,Jacquemart, D., Kopke,

P., Mandin, J.Y., Massie, S., Mikhailenko, S., Nemtchinov, V., Nikitin, A., Newnham, D., Perrin, A., Perevalov, V.I., Regalia-Jarlot, L., Rublev, A., Schreier, F., Schult, I., Smith, K.M., Tashkun, S.A., Teffo, J.L., Toth, R.A., Tyuterev, Vl. G.,Vander Auwera, Varanasi, J.P., Wagner, G.: The 2003 edition of the GEISA/IASI spectroscopic database, *J. Quant. Spectrosc. Radiat. Transfer*, **95**, 429-467, 2005.

Kara, A.B. and Barron, C.N.: Fine-resolution satellite-based daily sea surface temperatures over the global ocean. *Journal of Geophysical Research*, **112** , C05041, doi:10.1029/2006JC004021, 2007.

Lafferty, W.J., Solodov, A.M., Weber, A., Olson, W.B. and Hartman, J-M.: Infrared collision-induced absorption by N2 near 4.3 μm for atmospheric applications: measurements and empirical modelling, *Appl. Optics*, **35**, 5911-5917, 1996.

McNally, A.P. and Watts, P.D.: A cloud detection algorithm for high-spectral-resolution infrared sounders, *Q J Roy Meteorol Soc*, **129**, 3411-3423, 2003.

Matricardi, M.: RTIASI-4, a new version of the ECMWF fast radiative transfer model for the infrared atmospheric sounding interferometer, *ECMWF Research Dept. Tech. Memo*. 345, http://www.ecmwf.int/publications, 2003.

Matricardi, M., Chevallier, F., Kelly, G., and Thepaut, J.-N.: An improved general fast radiative transfer model for the assimilation of radiance observations, *Q. J. Roy. Meteorol. Soc*., **130**, 153-173, 2004.

Matricardi, M.: The inclusion of aerosols and clouds in RTIASI, the ECMWF fast radiative transfer model for the infrared atmospheric sounding interferometer, *ECMWF Research Dept. Tech. Memo*. 474, http://www.ecmwf.int/publications, 2005.

Matricardi, M.: An inter-comparison of line-by-line radiative transfer models, *ECMWF Research Dept. Tech. Memo*. 525, http://www.ecmwf.int/publications, 2007.

Matricardi, M.: The generation of RTTOV regression coefficients for IASI and AIRS using a new profile training set and a new line-by-line database, *ECMWF Research Dept. Tech. Memo*. 564, http://www.ecmwf.int/publications, 2008.

McNally, A.P., Watts, P.D., Smith, J.A., Engelen, R., Kelly, G.A., Thepaut, J.N., and Matricardi, M.: The assimilation of AIRS radiance data at ECMWF, *Q. J. Roy. Meteorol. Soc*., **132**, 935-957, 2006.

Niro, F., Jucks, K., and Hartmann, J.-M.: Spectra calculations in central and wing regions of CO_2 IR bands. IV: software and database for the computation of atmospheric spectra, *Journal of Quantitative Spectroscopy and Radiative Transfer*, **95**, Issue 4, 469-481, 2005.

Prinn, R.G., Weiss, R.F., Fraser, P.J., Simmonds, P.G., Cunnold, D.M., Alyea, F.N., O'Doherty, S., Salameh, P., Miller, B.R., Huang, J., Wang, R.H.J., Hartley, D.E., Harth, C., Steele, L.P., Sturrock, G., Midgley, P.M. and, McCulloch, A.: A History of Chemically and Radiatively Important Gases in Air deduced from ALE/GAGE/AGAGE, *J. Geophys. Res*., **105**, 17,751-17,792, 2000.

Rabier, F., Thepaut, J.-N., and Courtier, P.: Extended assimilation and forecast experiments with a four dimensional variational assimilation scheme, *Q. J. Roy. Meteorol. Soc*., **132**, 935-957, 1998.

Rinsland, C.P., Zander, J.S., Namkung, J.S., Farmer, C.B., and Norton, R.H.: Stratospheric infrared continuum absorption observed by the ATMOS instrument, *J. Geoohys, Res*., **94**, 16303-16322, 1989.

Rothman, L.S., Barbe, A., Chris Benner, D., Brown, L.R., Camy-Peyret, C., Carleer, M.R., Chance, K., Clerbaux, C., Dana, V., Devi, V.M., Fayt, A., Flaud, J.-M., Gamache, R.R., Goldman, A., Jacquemart, D., Jucks, K.W., Lafferty, W.J., Mandin, J.-Y., Massie, S.T., Nemtchinov, V., Newnham, D.A., Perrin, A., Rinsland, C.P., Schroeder, J., Smith, K.M., Smith, M.A.H., Tang, K., Toth, R.A., Vander Auwera , J., Varanasi, P., Yoshino, K.: The HITRAN molecular spectroscopic database: edition of 2000 including updates through 2001, *J. Quant. Spectrosc. Radiat. Transfer*, **82,** 5-44, 2003.

Rothman, L.S., Jacquemart, D., Barbe, A., Chris Benner, D., Birk, M., Brown, L.R., Carleer, M.R., Chackerian Jr., Chance, C.K., Coudert, L.H., Dana, V., Devi, V.M., Flaud, J.M., Gamache, R.R., Goldman, A., Hartmann, J.M., Jucks, K.W., Maki, A.G., Mandin, J.Y., Massie, S.T., Orphal, J., Perrin, A., Rinsland, C.P., Smith, M.A.H., Tennyson, J., Tolchenov, R.N., Toth, R.A., Vander Auwera, J., Varanasi, P., Wagner, G.: The HITRAN 2004 molecular spectroscopic database, *J. Quant. Spectrosc. Radiat. Transfer*, **96,** 139-204, 2005.

Saunders, R., Matricardi, M. and Brunel, P.: An improved fast radiative transfer model forassimilation of satellite radiance observations, *Quart. J. Roy. Meteor. Soc.*, **144**, 1547-1558, 1999.

Saunders, R., Matricardi, M., and Geer, A.: RTTOV9.1 users guide, *NWP SAF report*, Met. Office, 57pp., 2008.

Masiello, G., Serio, C., Carissimo, A., Grieco, G., and Matricardi, M.:Application of φ-IASI to IASI: retrieval products evaluation and radiative transfer consistency, *Atmos. Chem. Phys*., in review, 2009.

Smith, W. L., Woolf, H. M., Hayden, C.M., Wark, D. Q., and McMillin, L.M.: The TIROS-N Operational Vertical Sounder. *Bull. Am. Meteorol. Soc*., **60**, 1177-1187, 1979.

Strow, L.L., Tobin, D.C., and Hannon, S.E.: A compilation of First-Order Line-Mixing coefficients for CO_2 Q-branches. *J. Quant. Spectrosc. Radiat. Transfer,* **52**, 281, 1994.

Strow, L. L., Motteler, H.E., Benson, R.G., Hannon, S.E., and De Souza-Machado, S.: Fast computation of monochromatic infrared atmospheric transmittances using compressed lookup tables, *J. Quant. Spectrosc. Radiat. Transfer*, **59**, 481-493, 1998.

Strow, L.L., Hannon, S.E., De Souza-Machado, Motteler, S.H., and Tobin, D.: An Overview of the AIRS Radiative Transfer Model, *IEEE Transactions on GeoSciences and Remote Sensing*, **41**, 274, 2003.

Tibault, F., Menoux, V., Le Doucen, R., Rosenman, L., Hartman, J.-M., and Boulet, Ch.: Infrared collision induced absorption by O2 near 6.4 microns for atmospheric applications: measurements and empirical modeling, *Appl. Optics*, **36**, 563-567, 1997.

Timofeyev, Y.M., and Tonkov, M.V.: Effct of the induced Oxygen absorption band on the transformation of radiation in the 6 μm region of the Earth's atmosphere, Izvestiya, *Atmospheric and Ocean Physics* **14**, 437-441, 1978.

Tobin, D.C.: *Infrared spectral lineshapes of water vapour and carbon dioxide*, Ph.D. dissertation, Univ. Maryland Baltimore County, Baltimore, MD, 1996.

Tobin, D.C., Best, F.A., Brown, P.D., Clough, S.A., Dedecker, R.G., Ellingson, R.G., Garcia, R.K., Howell, H.B., Knuteson, R.O., Mlawer, E.J., Revercomb, H.E., Short, J.F., van Delst, P.F.W., and Walden, V.P.: Downwelling spectral radiance observations at the SHEBA ice station: Water vapor continuum measurements from 17 to 26 μm, *J. Geophys. Res*., **104**, 2081-2092, 1999.